

very much like tachyons and antitachyons.

The Frenkel-Kontorova model might be quite useful for studying the stability and the interactions of tachyons, and tardons as well, for that matter. It might possibly provide the key to an explanation of why tachyons are impossible.

In the present model, a tachydislocation is described by a chain of atoms in which most of the atoms sit on potential crests. At dislocation speeds only moderately exceeding the speed of sound, and at low dislocation densities, such states are not stable against small perturbations.⁵ It remains to be shown whether or not stability can be re-established at high speeds and densities. At any rate, tachydislocations have not been observed so far.

It should be pointed out that the relativistic expression for the energy of a tachydislocation is obtained only after subtracting the maximum potential energy of the chain. This term is, of course, infinite for an infinite chain. In an otherwise normal chain, a finite region where tachydislocations could exist would be excited to a high energy. Consequently, the region would be observed as a massive object. This would fit the "rigid wall" picture, in one dimension at least.

Moreover, if we divide the chain into two semi-infinite regions carrying tardons and tachyons, respectively, then the boundary between the two regions must travel at the speed of light since it

is at the same time a tachyon and a tardon. Thus it appears that, in a one-dimensional universe at least, tachyons could exist only in limited regions which should be inaccessible to tardons.

Consequently, this model yields an indication, though certainly not a proof, that tachyons are unlikely to occur.

Finally, it should be noted that one obtains a more realistic, though somewhat awkward, picture of a particle in two or three dimensions by repeated application of the Frenkel-Kontorova model in perpendicular directions. Sanders⁶ worked out such a model to describe a dislocation kink.

¹O. M. P. Bilaniuk, V. K. Deshpande, and E. C. G. Sudarshan, *Am. J. Phys.* **30**, 718 (1962).

²O. M. Bilaniuk and E. C. G. Sudarshan, *Phys. Today* **22**, No. 5, 43 (1969).

³O. M. Bilaniuk, S. L. Brown, B. DeWitt, W. A. Newcomb, M. Sachs, E. C. G. Sudarshan, and S. Yoshikawa, *Phys. Today* **22**, No. 12, 47 (1969).

⁴T. Kontorova and Ya. I. Frenkel, *Zh. Eksperim. i Teor. Fiz.* **8**, 89 (1938). For quick reference consult F. R. N. Nabarro, *Theory of Crystal Dislocations* (Oxford Univ., London, 1967), §3.2, p. 130, and §7.1.1.2, p. 489.

⁵F. C. Frank and J. H. van der Merwe, *Proc. Roy. Soc. (London)*, Ser. A **201**, 261 (1950).

⁶W. T. Sanders, *J. Appl. Phys.* **36**, 2822 (1965) and *Phys. Rev.* **154**, 654 (1967).

PHOTOPRODUCTION OF ω MESONS FROM COMPLEX NUCLEI*

H.-J. Behrend, F. Lobkowicz, E. H. Thorndike, and A. A. Wehmann†

Department of Physics and Astronomy, University of Rochester, Rochester, New York 14627

and

M. E. Nordberg, Jr.

Laboratory of Nuclear Studies, Cornell University, Ithaca, New York 14850

(Received 25 March 1970)

Photoproduction of ω mesons from Be, C, Al, Cu, and Pb has been studied at a mean energy of 6.8 GeV. The t distributions show a forward peak characteristic of a coherent diffraction mechanism, but also a considerable cross section at large t characteristic of an incoherent production mechanism. The ratio of cross sections for coherently photo-produced ρ^0 mesons to ω mesons is 11.8 ± 1.3 compared with the simple SU(3) prediction of 9.

There have been extensive experimental studies of the photoproduction of ρ^0 mesons from complex nuclei,^{1,2} and some studies of φ photoproduction.³ Similar experiments for ω mesons have been lacking until now because of the technical difficulties in detecting either of the two strongest

decay modes ($\pi^+\pi^-\pi^0$ or $\pi^0\gamma$). The only measurements available so far have been carried out in a hydrogen bubble chamber at energies between 2 and 6 GeV.^{4,5} They showed a cross section decreasing with energy suggesting that there is, besides the diffraction production process, an

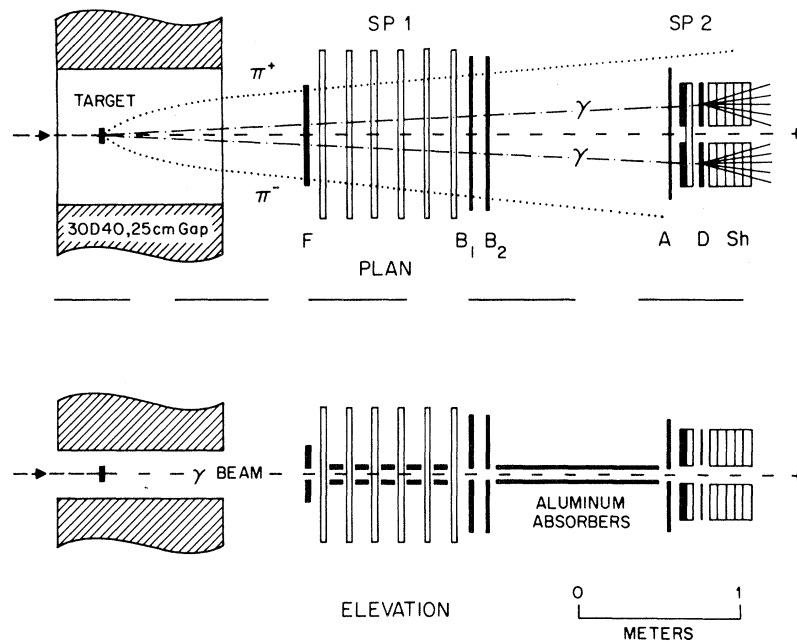


FIG. 1. Geometry of the apparatus used for detecting photoproduced ω mesons through their decay $\pi^+\pi^-\pi^0$. For a detailed description of the equipment, see text. The two spark chamber setups SP1 and SP2 with their associated counters could be moved independently up and down on precision jacks.

appreciable contribution of at least one other energy-dependent production mechanism, presumably a one-pion exchange process. Omega production on complex nuclei can lead to a separation of the diffraction process and can give information on the ωN total cross section $\sigma_{\omega N}$ and the $\gamma\omega$ coupling constant. This Letter presents a first survey of ω photoproduction from complex nuclei.

The apparatus used in this experiment is shown in Fig. 1. A 9.2-GeV bremsstrahlung beam, produced in an internal target of the 10-GeV Cornell electron synchrotron, was hardened by a 1-m LiH hardener and collimated to a size 0.5×1 cm at the target. The target was inside a dipole magnet with a 25-cm gap, 75-cm width, and 100-cm length. The photoproduced ω mesons were detected through the dominant decay mode $\omega \rightarrow \pi^+\pi^-\pi^0$. The charged pions were measured in a wire-chamber array SP1 located downstream of the magnet. The x -coordinate wires of the first two chambers were rotated by 15° from the vertical, thus enabling a correlation of the two views of each track. All chambers had a dead region in the median plane so that the γ beam and electron pairs produced in the target did not pass through their sensitive region. Aluminum absorbers above and below the beam between the chambers reduced low-energy background. Four

trigger counters F in symmetric quadrants in front of the spark chamber array and four pairs of counters B_1, B_2 in back registered the presence of charged pions.

The γ rays from the π^0 decay passed through the charged-pion detecting apparatus and an array of anti-counters A and were then converted in $1\frac{1}{2}$ radiation lengths of lead. Their position and energy were measured in a spark-chamber-counter combination consisting of four identical quadrants. Each converted γ ray was detected in a counter D , located between the lead converter and the shower counter. Its position was measured in a strip spark-chamber array⁶ SP2. The energy was determined in a shower counter consisting of lead plates immersed in a liquid scintillator and viewed by a large photomultiplier. A 7.5-cm gap in the median plane was left free of material in order to prevent background from the γ beam and electron pairs produced in the target. The probability that both γ rays are converted was calculated to be $(52 \pm 1)\%$.

The system was triggered by detection of two charged particles in the F and B counters simultaneously with two γ rays. The wire and strip spark chambers had magnetostrictive readout. The information from the spark chambers and shower-counter pulse heights was digitized and read into an IBM 1800 computer, which performed

on-line consistency checks and wrote the data on magnetic tape.

The performance of the detection system was extensively tested with photoproduction of e^+e^- pairs and ρ^0 mesons at varying intensities, as well as with the direct γ beam. The absolute detection efficiency for charged pion pairs in the spark chambers SP1 was $(97.5 \pm 1)\%$ at low intensities, and the intensity losses were $\leq 5\%$ and known to $\pm 2\%$. The strip chambers recording the γ position (SP2) had an efficiency of $(89 \pm 2)\%$ per converted γ quantum. The shower counters were calibrated with electron pairs of energy measured in SP1. The geometric efficiency (effective solid angle) of the experimental setup was determined by a detailed Monte Carlo study. The detection efficiency varied typically from 0.05% for 5-GeV/c ω mesons to 0.25% for 8-GeV/c mesons and was known to 5% of its value.

The γ -beam intensity during data taking was typically 10^7 quanta/sec. The trigger rate varied from element to element in the range (0.5-5)/min. Target thicknesses were limited by multiple scattering and by the necessity of limiting the electromagnetic background; they were in the range of 0.04-0.08 radiation lengths.

For the final analysis, the π^0 mass was first reconstructed from the γ -ray energies and directions [see Fig. 2(a)]. If the π^0 mass was within the allowed range, the π^0 momentum was deter-

mined using the known π^0 mass as an additional constraint, thus reducing the sensitivity to the rather crude determination of γ -ray energies. The charged-pion momenta were determined by reconstructing their tracks in the chamber array SP1 and tracing their path back to the target. From the pion momenta we determine the ω mass and momentum and its decay parameters. The 3π invariant-mass spectrum in Fig. 2(b) shows clearly a peak at the ω mass and a background which consists mainly of nonresonant $\pi^+\pi^-\pi^0$ events. All ω mesons without energy cut were accepted for calculating the differential cross sections. Because of the energy dependence of the efficiency most events were in the region 6-9 GeV. The distribution of the events in momentum space as well as in physical space was compared in detail with the Monte Carlo prediction. In general, excellent agreement was found; in particular, the normal to the decay plane (in the ω center-of-mass system) showed the expected $\sin^2\theta$ distribution on the helicity frame for the small-angle events [$|t| < 0.1$ (GeV/c) 2], as shown in Fig. 2(c).

Some of the corrections to the data due to finite γ -conversion efficiency, effective solid angle, and finite chamber efficiencies have been discussed earlier. Corrections were also applied for γ -ray and charged-pion absorption in the target and detection equipment [(30 \pm 2) %], ω branching ratio (10 %), counter inefficiencies and dead times (4 %), charged-pion decay (3 %), and events lost due to kinematical and mass cuts (8 %). The background under the mass peak in Fig. 2(b) was subtracted by assuming that its t distribution was the same as for the $\pi^+\pi^-\pi^0$ events whose mass is close to, but different from, the ω mass.

The differential cross sections $d\sigma/dt$ for beryllium and copper are shown in Fig. 3(a). While there is a clearly distinguishable diffractive forward peak, there is also a contribution from non-diffractive processes, especially in light nuclei. These nondiffractive processes are 2 to 3 times larger in ω photoproduction than in ρ photoproduction.^{2,7} This is to be expected, since one-pion exchange (OPE) processes are considerably more important in ω photoproduction. OPE will give rise to two nondiffractive processes: (i) Inelastic photoproduction, where additional pions are produced in the reaction. The main contribution should be from the reaction $\gamma N \rightarrow \omega N^*(1238)$ on one of the nucleons. (ii) Incoherent photoproduction, in which the final nuclear state is not the ground state (and may lead to breakup of the nu-

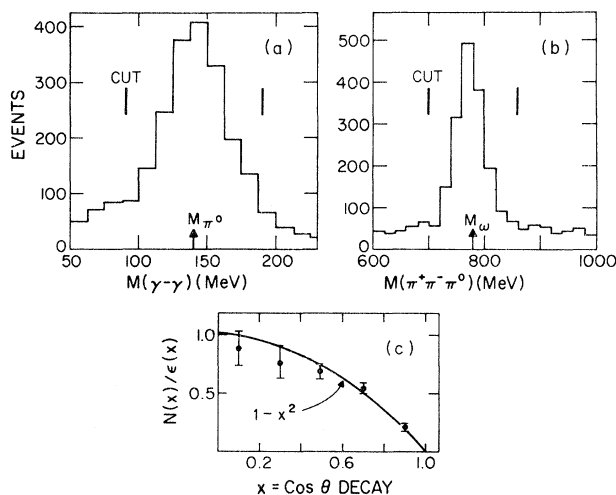


FIG. 2. (a) Invariant-mass distribution of the two detected γ rays. (b) Invariant-mass distribution of $\pi^+\pi^-\pi^0$, after a mass cut has been applied to the invariant 2γ mass. (c) Distribution in $\cos\theta_{\text{decay}}$ for ω mesons produced with $|t| < 0.1$ (GeV/c) 2 . Here θ_{decay} is the polar angle of the normal to the decay plane in the helicity frame.

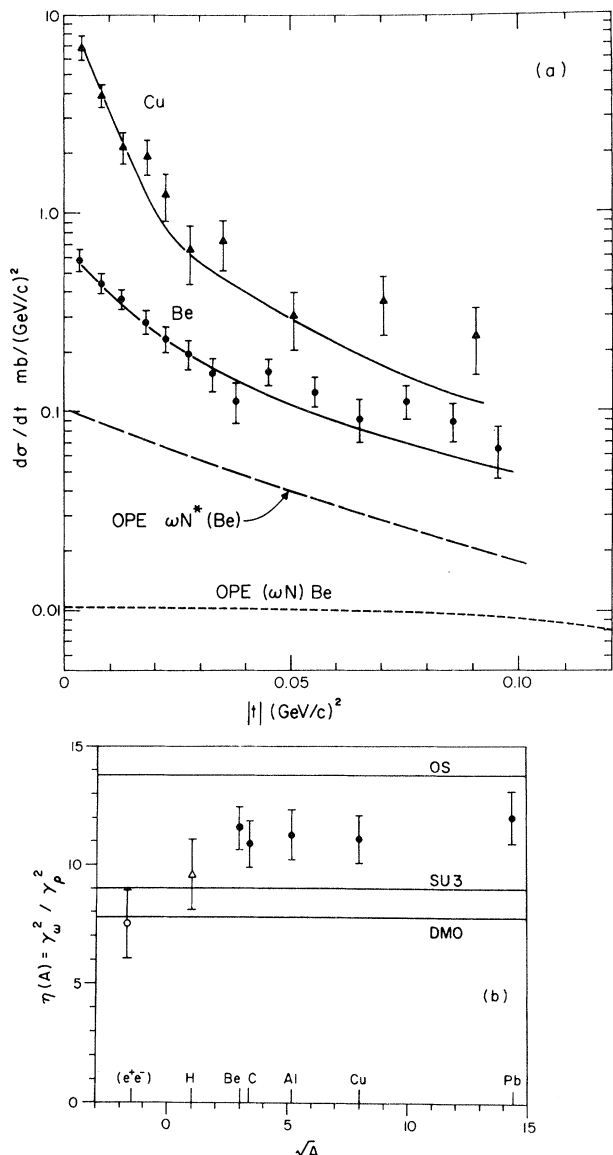


FIG. 3 (a) Differential cross sections for ω photoproduction in beryllium and copper. The two dashed lines indicate the contributions given by the two terms in Eq. (1) for beryllium. The solid lines are fits to the data given by Eq. (2). (b) Closed circles: the ratio $\eta(A) = (d\sigma/dt)_{\gamma A \rightarrow \rho A} [(d\sigma/dt)_{\gamma A \rightarrow \omega A}^{\text{Diff}}]^{-1}$ obtained from the fits using Eq. (2). Open triangle: the ratio of total diffractive photoproduction cross sections of ρ and ω mesons on hydrogen, as given by Ref. 5. Open circle: $\gamma_{\omega}^2/\gamma_{\rho}^2$ as determined from colliding-beam experiments. The horizontal solid lines denote theoretical predictions discussed in the text.

cleus), but no pions are produced.

The contribution of inelastic and incoherent events was calculated using the following expression:

$$\left(\frac{d\sigma}{dt}\right)^{\text{OPE}} = A_{\text{eff}} \left[\left(\frac{d\sigma}{dt^*}\right)_{\omega N^*} + G(t) \left(\frac{d\sigma}{dt}\right)_{\omega N} \right]. \quad (1)$$

Here A_{eff} is the effective number of nucleons contributing to incoherent photoproduction; its value was taken as obtained from large-angle ρ^0 photoproduction⁷ and π^+ photoproduction⁸ in complex nuclei. $(d\sigma/dt^*)_{\omega N^*}$ and $(d\sigma/dt)_{\omega N}$ are cross sections for the processes $\gamma N \rightarrow \omega N^*(1236)$ and $\gamma N \rightarrow \omega N$ calculated by Wolf using an OPE model.⁹ The cross section for $\gamma N \rightarrow \omega N^*$ was taken at a different value t^* to take into account that in this experiment the momentum transfer was reconstructed assuming elastic photoproduction. Finally, $G(t)$ is a correction factor calculated by von Bochmann, Margolis, and Tang¹⁰ to take into account the suppression of incoherent processes at small t because of nuclear correlations.¹¹ The long- and short-dashed lines in Fig. 3(a) indicate the relative importance of the elastic and the incoherent contribution to $(d\sigma/dt)^{\text{OPE}}$.

The solid lines in Fig. 3(a) are obtained by fitting

$$\begin{aligned} \left(\frac{d\sigma}{dt}\right)_{\omega A} &= \left(\frac{d\sigma}{dt}\right)_{\omega A}^{\text{Diff}} + \left(\frac{d\sigma}{dt}\right)_{\omega A}^{\text{OPE}} \\ &= \frac{1}{\eta(A)} \left(\frac{d\sigma}{dt}\right)_{\rho A} + \left(\frac{d\sigma}{dt}\right)_{\omega A}^{\text{OPE}}, \end{aligned} \quad (2)$$

where $(d\sigma/dt)^{\text{OPE}}$ is taken from Eq. (1), $(d\sigma/dt)_{\rho A}$ is the measured photoproduction cross section of ρ^0 mesons on the same nucleus, and $\eta(A)$ is a fitting parameter which gives the ratio between diffractive ρ^0 and ω photoproduction cross sections.¹² Assuming the same nuclear parameters for both processes, this procedure gives the most accurate determination of the ratio of the two reactions. The value of η as a function of A is shown in Fig. 3(b). The errors include statistical errors as well as a 10% uncertainty in the OPE cross sections and uncertainties in the assumption of A_{eff} . An additional 10% overall normalization uncertainty is not included in the errors.

The diffractive contribution to ω photoproduction can be expressed at small angles, where coherent production dominates, as

$$\left(\frac{d\sigma}{dt}\right)_{\omega A}^{\text{Diff}} = \left(\frac{d\sigma}{dt}\right)_{\omega N} f(R_A, \sigma_{\omega N}, \alpha_{\omega N}, t), \quad (3)$$

where $(d\sigma/dt)_{\omega N}$ is the diffractive photoproduction cross section on hydrogen, and where $f(R, \sigma, \alpha, t)$ is a function of the nuclear radius R_A , the ω -nucleon total cross section $\sigma_{\omega N}$, and the ratio $\alpha_{\omega N}$ of the real to the imaginary part of the ω -nucleon forward scattering amplitude.¹³ Since the same expression holds for ρ^0 photoproduction, the near constancy of $\eta(A)$ suggests that $\sigma_{\omega N} \cong \sigma_{\rho N}$ and $\alpha_{\omega N}$

$\cong \alpha_{\rho N}$. We have analyzed our data by assuming that $\alpha_{\omega N} = \alpha_{\rho N} = -0.2$, and searching for $\sigma_{\omega N}$ and $(d\sigma/dt)_{\omega N}$. The result is

$$\begin{aligned}\sigma_{\omega N} &= 33.5 \pm 5.5 \text{ mb}, \\ (d\sigma/dt)_{\omega N} &= 11.4 \pm 1.9 \text{ } \mu\text{b/GeV}^2.\end{aligned}\quad (4)$$

Under the assumption of vector-meson dominance this leads to a value of the $\gamma\omega$ coupling constant $\gamma_{\omega^2}/4\pi = 9.5 \pm 2.1$.

The quark model¹⁴ predicts $\sigma_{\omega N} = \sigma_{\rho N}$ and $\alpha_{\omega N} = \alpha_{\rho N}$. Since the value of $\sigma_{\omega N}$ obtained in this experiment is quite consistent with this hypothesis, one can set, in addition, $\sigma_{\omega N} = \sigma_{\rho N} = 27 \pm 2$ mb and thus obtain a more accurate result:

$$\begin{aligned}(d\sigma/dt)_{\omega N} &= 9.6 \pm 1.2 \text{ } \mu\text{b/GeV}^2, \\ \gamma_{\omega^2}/4\pi &= 7.3 \pm 1.0.\end{aligned}\quad (5)$$

The error is mainly due to the 10% uncertainty in absolute normalization in this experiment. Assuming the quark-model hypothesis and identical nuclear physics, the ratio $\eta(A)$ plotted in Fig. 3(b) can be regarded as $\gamma_{\omega^2}/\gamma_{\rho^2}$.

Our value given by Eq. (5) is in significant disagreement with the value $\gamma_{\omega^2}/4\pi = 3.7 \pm 0.7$ obtained by colliding e^+e^- beam measurements.¹⁵ The original SU(3) prediction of $\gamma_{\omega^2}/\gamma_{\rho^2} = 9:1$ has been modified by Das, Mathur, and Okubo¹⁶ (DMO) and by Oakes and Sakurai¹⁷ (OS). The predicted values are $\gamma_{\omega^2}/\gamma_{\rho^2} = 7.6$ (DMO) and 13.8 (OS), respectively. The results of colliding-beam experiments¹⁸ are 7.5 ± 1.5 . This is to be compared with our value of 11.8 ± 1.3 . Thus, while the storage-ring results give good agreement with DMO and SU(3), our result falls halfway between OS and SU(3) and is inconsistent with DMO. We note here that there seems to be a general tendency for $\gamma_{\omega^2}/4\pi$ to be larger in photoproduction than if determined from colliding beam experiments.¹⁹

The authors gratefully acknowledge the support and continuing interest of Professor B. D. McDaniel and thank him for his hospitality to the Rochester group during their stay at Cornell. Dr. M. Tigner and the synchrotron operating crew are due grateful recognition for the flawless performance of the accelerator. Professor L. Hand and Mr. T. Loomis participated in the early stages of the experiment. We thank Dr. G. Wolf for performing the OPE calculations used in this experiment. Mr. C. K. Lee, Mr. J. Abramson, Mr. J. Harvey, Mr. E. May, and Mr. M. Singer helped during the running and analysis of the experiment.

*Research supported by the National Science Foundation.

†Present address: National Accelerator Laboratory, P. O. Box 500, Batavia, Ill. 60501.

¹H. Blechschmidt *et al.*, Nuovo Cimento **52A**, 1348 (1967); G. McClellan *et al.*, Phys. Rev. Letters **22**, 377 (1969); F. Bulos *et al.*, Phys. Rev. Letters **22**, 490 (1969); H. Alvensleben *et al.*, DESY Report No. 69/50, 1969 (unpublished).

²H.-J. Behrend *et al.*, Phys. Rev. Letters **24**, 336 (1970).

³G. McClellan *et al.*, Cornell Univ. Report No. CLNS-70; S. C. C. Ting, in *Proceedings of the Fourteenth International Conference on High Energy Physics, Vienna, Austria, September 1968*, edited by J. Prentki and J. Steinberger (CERN Scientific Information Service, Geneva, Switzerland, 1968).

⁴Aachen-Berlin-Bonn-Hamburg-Heidelberg-München Collaboration, Phys. Rev. **175**, 1669 (1968); Brown-Harvard-M.I.T.-Padova-Weizmann Institute Bubble Chamber Collaboration, Phys. Rev. **155**, 1468 (1967).

⁵G. Wolf [Bull. Am. Phys. Soc. **15**, 99 (1970)] gives a total diffractive ω -photoproduction cross section of 1.8 ± 0.2 mb at 4.7 GeV. We note here that they obtain a ρ^0 photoproduction cross section on hydrogen different from the value given by Alvensleben *et al.*, Ref. 1. We use an average of the older values for our comparison.

⁶These chambers consisted of 1-cm-wide copper strips instead of wires, thus preventing a shower from causing too many small sparks. Their construction and performance is described in M. E. Nordberg, Jr., *et al.*, to be published.

⁷G. McClellan *et al.*, Phys. Rev. Letters **23**, 554 (1969). Nondiffractive production means that the final nuclear state is different from the initial one. The process still can be dominated by diffractive scattering off single nucleons, as is the case for ρ^0 photoproduction.

⁸A. M. Boyarski *et al.*, Phys. Rev. Letters **23**, 1343 (1969). We take A_{eff}/A as equal to Z_{eff}/Z .

⁹G. Wolf, Phys. Rev. **182**, 1588 (1969), and private communication. The same calculation describes well the unnatural-parity-exchange cross section for the reaction $\gamma + p \rightarrow \omega + p$, as recently measured by the SLAC bubble chamber group, as well as a measurement of ω photoproduction on hydrogen and deuterium done by us with the same equipment. See also Ref. 5.

¹⁰G. von Bochmann, B. Margolis, and L. C. Tang, Phys. Letters **30B**, 254 (1969); B. Margolis, private communication.

¹¹There is no corresponding suppression of inelastic photoproduction.

¹²Data of Ref. 2 were used for this fit. The slightly different t resolution in the two experiments was taken into account for the heavier nuclei. Small corrections were applied to take into account the large range of energies accepted in this experiment.

¹³The complete description of $f(R, \sigma, \alpha, t)$ is given, e.g., in Behrend *et al.*, Ref. 2. The same nuclear density distributions were used here.

¹⁴Since $m_p \approx m_n$, this equality is independent of whether one compares hadron cross sections at equal energy or equal relative velocity. Compare P. B. James and H. D. D. Watson, *Phys. Rev. Letters* **18**, 179 (1966); S. A. Jackson and R. E. Mickens, to be published.

¹⁵J. E. Augustin *et al.*, *Phys. Letters* **28B**, 513 (1969).

¹⁶T. Das, V. S. Mathur, and S. Okubo, *Phys. Rev. Letters* **19**, 470 (1967).

¹⁷R. J. Oakes and J. J. Sakurai, *Phys. Rev. Letters* **19**, 1266 (1967).

¹⁸J. Perez-y-Jorba, in *Proceedings of the Fourth*

International Symposium on Electron and Photon Interactions at High Energies, Liverpool, England, September 1969, edited by D. W. Braben (Daresbury Nuclear Physics Laboratory, Daresbury, Lancaster, England, 1969).

¹⁹A. S. Silverman, in *Proceedings of the Fourth International Symposium on Electron and Photon Interactions at High Energies, Liverpool, England, September, 1969*, edited by D. W. Braben (Daresbury Nuclear Physics Laboratory, Daresbury, Lancaster, England, 1969); and Perez-y-Jorba, Ref. 18.

$\bar{p}n$ ELASTIC SCATTERING FROM $-t=0.15$ TO 1.0 (GeV/c)² AT 3.5 GeV/c*

B. G. Reynolds, K. E. Weaver, J. M. Bishop, D. O. Huwe, and J. A. Malko
Department of Physics, Ohio University, Athens, Ohio 45701

(Received 29 December 1969)

We have measured the $\bar{p}n$ differential elastic cross section in the four-momentum-transfer region of $-t=0.15$ to 1.0 (GeV/c)² using neutron scatters obtained in a $\bar{p}d$ bubble chamber experiment at 3.5 GeV/c. The $\bar{p}n$ elastic cross section is similar to the $\bar{p}p$ cross section at this energy to the extent that both cross sections exhibit a diffraction peak and a dip at $-t \approx 0.45$ followed by a secondary peak. A comparison of $\bar{p}n$ and $\bar{p}p$ elastic scattering indicates a crossing of the two cross sections near the region of the dip. The results of this experiment suggest the presence of an $I=1$, t -channel exchange in $\bar{N}N$ scattering.

Several studies of $\bar{p}p$ elastic scattering above 2 GeV/c have been made during the past several years.¹⁻⁶ Corresponding studies of $\bar{p}n$ elastic scattering are noticeably absent and our main interest in studying $\bar{p}n$ elastic scattering was to compare our results with $\bar{p}p$ scattering. Recent evidence suggests that $\bar{N}N$ elastic scattering is dominated by $I=0$ meson exchange for small four-momentum transfer and laboratory momenta above 1.5 GeV/c.⁷ Since the $I=1$ exchange amplitude contributes to the total $\bar{p}p$ and $\bar{p}n$ elastic scattering amplitudes with a difference in sign, it is not unreasonable to expect that the presence of an $I=1$ exchange amplitude might show up as a difference between the $\bar{p}p$ and the $\bar{p}n$ elastic-scattering cross sections. Differences in the two cross sections have been reported in the region of 1.65 GeV/c.⁷ In this Letter we present our data and make a comparison with $\bar{p}p$ elastic scattering at 3.55 GeV/c.¹

The data for this experiment were obtained from an exposure of the deuterium-filled 30-in. MURA bubble chamber at Argonne National Laboratory to a beam of 3.5 -GeV/c antiprotons. In order to avoid the ambiguity of target that is present for small-angle scattering in deuterium, it was necessary to exclude the small-angle scatters by placing restrictions on spectator proton range and on the projection of the laboratory

scattering angle of the antiproton onto the film plane. Since the scattering angle and the proton range are only correlated in $\bar{p}p$ scatters, we selected cutoff values for these quantities such that it was highly unlikely that the antiproton was scattered by a proton. The angle φ actually observed in scanning an event was not the scattering angle but the angle defined by the beam track and projection of the outgoing antiproton track onto the film plane. As such, this angle is always less than or equal to the laboratory scattering angle. For this experiment we required that proton range be ≤ 2.0 cm. This limit corresponds to a proton momentum ≤ 180 MeV/c. The requirement on φ was $\varphi \geq 5^\circ$. The 5° limit corresponds to a value of $-t$, the four-momentum-transfer squared, ≥ 0.1 (GeV/c)². This requirement on φ introduces a bias against events whose scattering plane dips with respect to the plane defined by the top of the chamber. The corrections for this bias are discussed below.

After geometric reconstruction and fitting, a cut at $-t=0.15$ (GeV/c)² was imposed and the contamination due to the $\bar{p}p$ and $\bar{p}d$ elastic scatters was estimated to be less than 10%. The major portion of this contamination as well as contamination due to spurious fits to inelastic events was eliminated by requiring the events to satisfy the kinematics of equal-mass scattering